Earthquakes and Structures, *Vol. 30, No. 5 (2020)000-000*
DOI: https://doi.org/10.12989/eas.2020.30.5.000

Seismic performance of high strength steel frames with variable eccentric braces based on PBSD method

Shen L[*1], Ze-yu Wang[1a], Hong-chao Guo[1b] and Xiao-lei Li[2c]

[1]*School of Civil Engineering and architecture, Xi'an University of Technology, Xi'an 710048, China*
[2]*State Key Laboratory Base of Eco-hydraulic Engineering in Arid Area, Xi'an University of Technology, Xi'an 710048, China*

(Received June 26, 2019, Revised October 25, 2019, Accepted November 18, 2019)

Abstract. In traditional eccentrically braced steel frames, damages and plastic deformations are limited to the links and the main structure members are required tremendous sizes to ensure elasticity with no damage based on the force-based seismic design method, this limits the practical application of the structure. The high strength steel frames with eccentric braces refer to Q345 (the nominal yield strength is 345 MPa) steel used for links, and Q460 steel utilized for columns and beams in the eccentrically brace steel frames, the application of high strength steels not only brings out better economy and higher strength, but also wider application prospects in seismic fortification zone. Here, the structures with four type eccentric braces are chosen, including K-type, Y-type, D-type and V-type. These four types EBFs have various performances, such as stiffness, bearing capacity, ductility and failure mode. To evaluate the seismic behavior of the high strength steel frames with variable eccentric braces within the similar performance objectives, four types EBFs with 4-storey, 8-storey, 12-storey and 16-storey were designed by performance-based seismic design method. The nonlinear static behavior by pushover analysis and dynamic performance by time history analysis in the SAP2000 software was applied. A total of 11 ground motion records are adopted in the time history analysis. Ground motions representing three seismic hazards: first, elastic behavior in low earthquake hazard level for immediate occupancy, second, inelastic behavior of links in moderate earthquake hazard level for rapid repair, and third, inelastic behavior of the whole structure in very high earthquake hazard level for collapse prevention. The analyses results indicated that all structures have similar failure mode and seismic performance.

Keywords: eccentrically braced steel frames; high strength steel; performance-based seismic design; seismic hazard

1. Introduction

Seismic resistant eccentrically braced frames (EBFs) are a lateral load-resisting system for steel buildings that combine high stiffness in the elastic range with good ductility and energy dissipation in the inelastic range. EBFs can be viewed as hybrid between concentrically braced frames (CBFs) and moment-resisting frames (MRFs). The bracing members in the EBFs provide the high elastic stiffness characteristic of the CBFs (Azad and Topkaya 2017). Yet, under the major earthquake, properly designed and detailed EBFs provide the ductility and energy dissipating capacity characteristic of MRFs. (Bosco and Rossi 2009, Dubina *et al*, 2010)

There are several configurations for an EBF system, some of which are depicted in Fig. 1 along with their expected plastic modes (Ashtari and Erfani 2016). The short segment of the frame generally designated by the length e is called the link. In EBF systems, yielding is concentrated only at link segments and all other members of the frame are proportioned to remain essentially elastic (Caprili *et al*. 2018). Therefore, during major earthquakes, links can be considered as structural fuses which will dissipate the seismic input energy through stable and controlled plastic deformations. However, in order to ensure the plastic deformations are limited to the links, the columns and beams are always overdesigned with limited or no damage. The traditional eccentrically braced frames are prone to over strength when designed by the force-based seismic method. Furthermore, we could not predict the overall failure mode of the structures under rare earthquakes using this traditional method. (Speicher and Iii 2016). The force-based seismic design method is very common and is found in most design codes, the traditional eccentrically braced steel frames are restricted in practical application due to poor economy. Nowadays, methods of seismic design are emphasizing more on performance-based seismic design concept to have a more realistic assessment of the inelastic response of the structure. (Di Trapani *et al*. 2018). The performance-based seismic design method can evaluate the performance objectives, failure modes, and reliability of structures (Castaldo *et al*. 2016).

The eccentrically braced frame structures fabricated with high strength steel (HSS-EBFs) are a new type of seismic structural system (Li *et al*. 2018, Lian *et al*. 2017, Wang *et*

*Corresponding author, Ph.D. Professor
E-mail: lishen2861@163.com
[a]Ph.D.
E-mail: lovemeyeh@qq.com
[b]Ph.D. Associate Professor
E-mail: ghc-1209@163.com
[c]Ph.D. Associate Professor
E-mail: lxl_832277@163.com

ISSN: 2092-7614 (Print), 2092-7622 (Online)

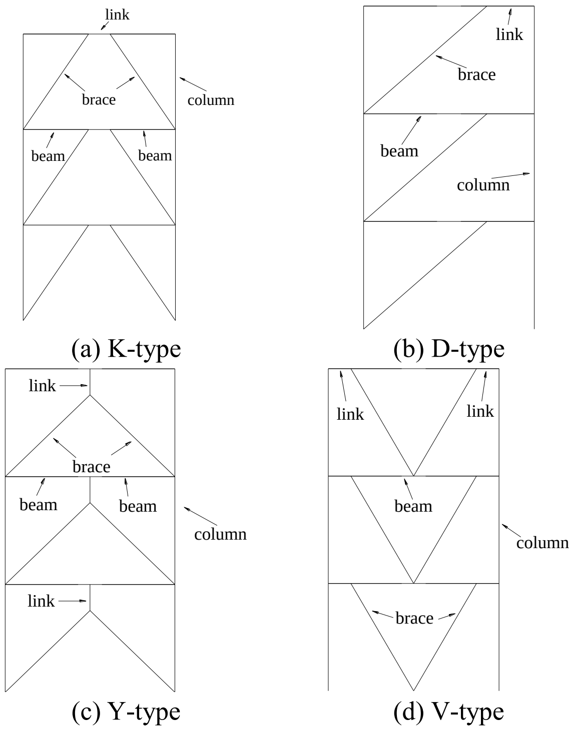

Fig. 1 Types of eccentrically braced frames

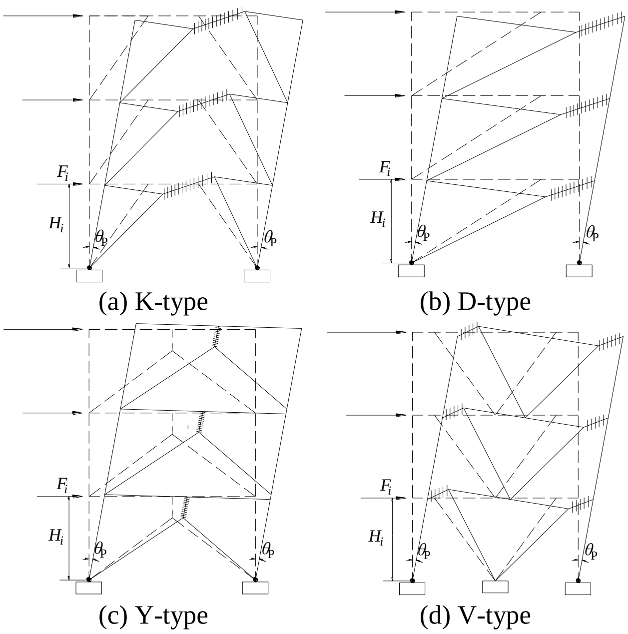

Fig. 2 Failure modes of eccentrically braced frames

al. 2016, Tian *et al*. 2018). HSS-EBFs systems can incorporate Q345 steel (The nominal yield strength is 345 MPa) for links, high strength steel (HSS) (The nominal yield strength not less than 460 MPa) for beams and columns, HSS-EBFs have good plastic deformation ability and ductility under rare earthquakes, while the main frame structure with high strength steel is basically in elastic. The use of high strength steel can effectively reduce the cross-section of components, at the same time reduce the use of anti-corrosion, fire-proof coatings, and increase usable area. However, the yield to strength ratio increases continuously and the elongation decrease gradually with the increase of steel strength. It is difficult for Q460 or higher strength steel to meet the mandatory requirements for steel in the Code for Seismic Design of Buildings in China (GB50011-2010), that is the ratio of yield strength to tensile strength should not be greater than 0.85, steel should have obvious yield steps and the elongation should not be less than 20%. The mandatory rules limit the application of high strength steel in seismic fortification areas. The HSS-EBFs can solve this problem well and promote the application of high strength steel in seismic zone. In this paper, four types of high strength steel frames with variable eccentric braces are designed by performance-based seismic design method. The links are made of Q345 steel, and the frame beams and columns are made of Q460 steel. The eccentric braces include K-type, Y-type, D-type and V-type. The prototype buildings include 4-storey, 8-storey, 12-storey and 16-storey. The performance-based design method can predict the distribution of shear force in the elastic-plastic state and the expected failure mode of the structures, which each link dissipate energy by plastic deformation under rare earthquakes, the story drift distributes evenly along the building height, and there are no weak story. In the ultimate state, the plastic hinge at the column base reaches the ultimate state. In this paper, pushover analysis and nonlinear dynamic analysis are used to study the seismic performance of EBFs with different braces.

2. Performance-Based Seismic Design (PBSD)

The target drift and expected failure mode were primarily determined when designed the structure through performance-based seismic design (PBSD) method. For EBFs, the expected failure mode refers to that only the links dissipate energy while the other components remain elastic when the structure being loaded in the elastic-plastic state. The story drifts along the height of the structure are well-distributed.

For EBFs, the process of PBSD method as following:

- Firstly, the fundamental period of EBFs structures is estimated and the yield drift θ_y and the target drift θ_u of EBFs are calculated by approximate formulas. And then the ductility factor $\mu_s=\theta_u/\theta_y$, and the ductility reduction factor R_μ is acquired by μ_s.
- Secondly, the base shear to structure weight ratio V/G under elastic-plastic state is calculated by ductility factor and other parameters, the base shear force under elastic-plastic state is obtained.
- Thirdly, the story shear force of each story is obtained via the shear force distribution under elastic-plastic state. β_i represents the shear distribution factor at level i, which is equal to V_i/V_n.
- And then, designs of links as a key procedure in the PBSD method, because of plastic deformations are isolated to links and column bases. In conditions where the distribution lateral force is known, yield shear links are proportioned to create uniform story drift along the structure height. By using the principle of virtual work and equating the external work to the internal work, the

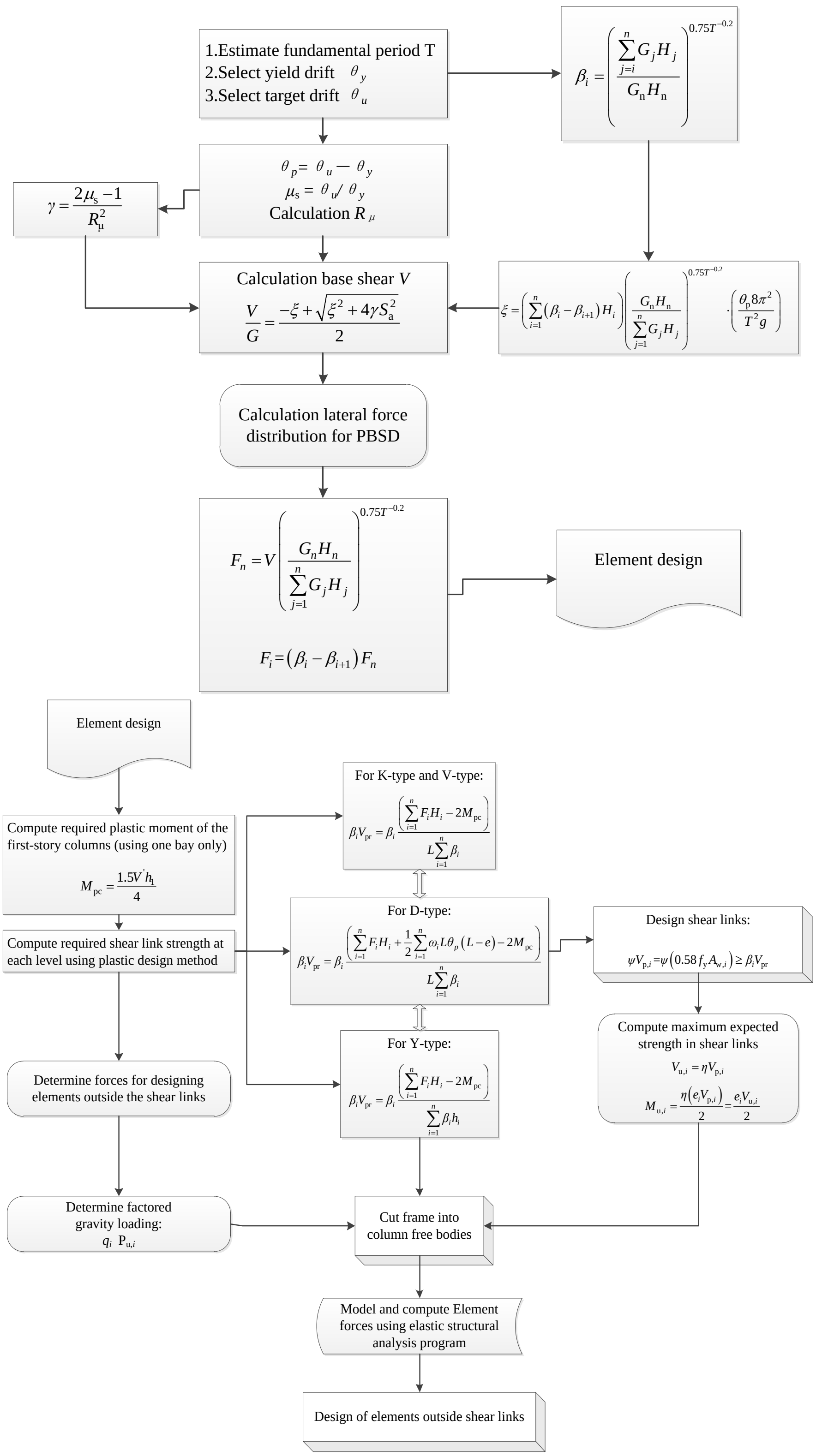

Fig. 3 Flow chart of PBSD method

section of shear links are determined.

• Finally, the other members, such as braces, beams and columns, are confirmed by the column free bodies using elastic structural design program.

The different types of HSS-EBFs were designed by performance-based seismic method have similar failure modes and performance objectives, as in this way, the seismic performance of different types of HSS-EBFs tend to be compared. The specific design process is shown in Fig. 3 (Li *et al*. 2017). Therefore, the different structures have the similar performance objectives, bearing capacity, failure mode, and story drift distribution.

Table 1 Member sizes for the specimen

Member	Section (Chinese designation)
Beam	H225×125×6×10
Column	H150×150×6×10
Brace	H125×120×6×10
Link	H225×125×6×10

Table 2 Mechanical properties of steel

Steel	Q345B	Q345B	Q460C	Q460C
Thickness t (mm)	6	10	6	10
Yield stress f_y (Mpa)	427.40	383.33	496.90	468.77
Ultimate strength f_u (Mpa)	571.10	554.40	658.57	627.97
Yield strain ε_y($\times10^{-3}$)	2.12	1.92	2.39	2.32
Elastic modulus E ($\times10^5$MPa)	2.01	2.00	2.08	2.02
Elongation ratio (%)	26.53	31.01	29.73	35.88

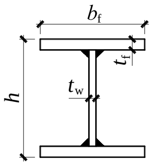

Fig. 4 Definition for the specimen sectional dimension

3. Experimental verification

3.1 Test preparation

A 1:2 scaled one-story one-bay K-type and Y-type HSS-EBF specimen with a shear link was designed and applied for the experimental study of its monotonic performance. The story height and span of the specimen were 1.8 and 3.6 m, respectively. The length of K-type shear link was 600 mm ($\rho=e/(M_p/V_p)=1.45$) and the length of shear links in Y-1 and Y-2 were 300 mm ($\rho=e/(M_p/V_p)=0.88$) and 500 mm ($\rho=e/(M_p/V_p)=1.46$), respectively; where, e, V_p, and M_p are the link length, plastic shear capacity, and plastic moment capacity, respectively), $\rho<1.6$, and the link is short (or shear yielding) in design.

Beams, columns, and braces were made of steel Q460 with nominal yield strength of 460 MPa, while the link was made of steel Q345 with nominal yield strength of 345 MPa. Welded joints were used to connect the link to the beam and the other members in the test specimen. The detailed member sections are listed in Table 1, the member sections are built-up section, and H-sections are used for the members, where "H" refers to the welded H-shaped section, the following numbers are section depth h, flange width b_f, web thickness t_w and flange thickness t_f, respectively (see Fig. 4) and the mechanical properties of the steel are presented in Table 2. The beam-column joint is a rigid connection, and the link and the frame beam are butt welded.

A vertical loading of 800 kN is applied to the top of the column by a hydraulic jack to simulate the axial force transferred to the column by the superstructure. The actuator is connected to the reaction wall at one end, and the specimen is connected at the other end to exert the horizontal load. The horizontal load is transferred to the frame column on the other side through the loading beam with the hinged connection and causes the synchronous lateral displacement of the frame on the left and right columns, thereby avoiding the influence of the transmission force of the link on the horizontal load transferring (Fig. 6). The test is monotonically loaded by the actuator at a loading speed of 0.05 mm/s until structural failure. The test setup in 3D view was shown in Fig. 7. To prevent lateral instability of the specimen, the specimen adopts four lateral bracings, which is connected with the beam of the specimen. The both ends of the lateral bracings are in contact with two smooth rigid panels, therefore, the lateral bracings and the specimen can move synchronously.

The arrangement of test displacement gauges is shown in Fig. 8. The displacement gauges measure two deformations, one is the horizontal displacement of the two columns of the specimen, and the other is the shear deformation of the link. Furthermore, the dial indicator is arranged to horizontal direction of the base platform in order to eliminate the slipping effect of base platform.

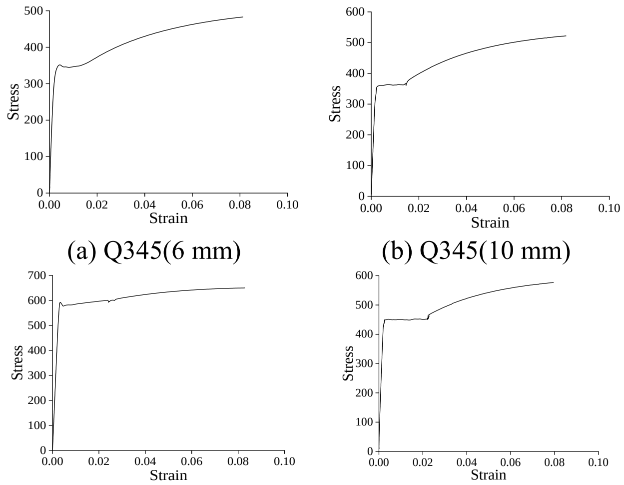

(a) Q345(6 mm) (b) Q345(10 mm)

(c) Q460(6 mm) (d) Q460(10 mm)

Fig. 5 Stress-strain curves

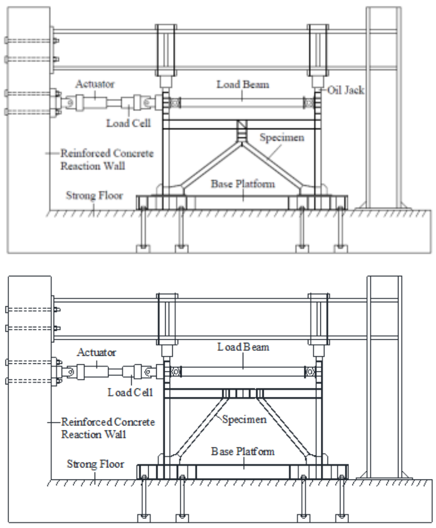

Fig. 6 Test setup

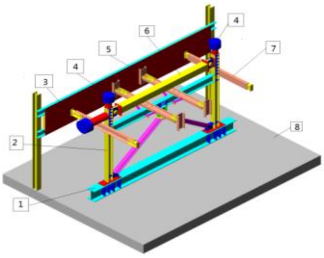

1. Base platform
2. Specimen
3. Actuator
4. Oil Jack
5. Rigid panel
6. Loading beam
7. Lateral bracing
8. Strong floor

Fig. 7 Test setups in 3D view

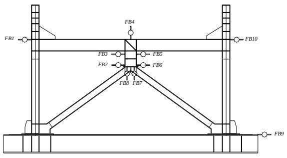

(a) Y-type EBFs specimen

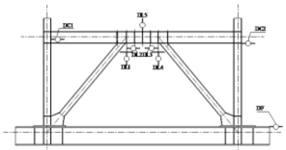

(b) K-type EBFs specimen

Fig. 8 Test displacement gauges

3.2 Test results

The pushover curves obtained by the monotonic loading of the specimen are shown in Fig. 9.

The monotonic test curves show that K-type and Y-type eccentrically braced structures exhibit excellent ductility and plastic deformation. The bearing capacity and stiffness of the specimens decreased with increasing plastic deformation of the link. The ultimate bearing capacity of K-type specimen is approximately 825 kN, and the corresponding ultimate story drift is 3.33%, which exceeds the limit of the elastic-plastic story drift, that is 2%. The ultimate bearing capacity of specimen Y-2 is approximately 730 kN, that is 7.4% greater than that of Y-1 (680 kN), and the corresponding ultimate displacements are 107.7 mm and 108.3 mm, respectively. The bearing capacity and stiffness of the specimens decreased with increasing link length. The structure has excellent deformation capacity and ductility.

The failure modes of the specimens from the monotonic test are shown in Figs. 10, 11 and 12. K-type and Y-type eccentrically braced steel frames with HSS structures dissipate seismic energy primarily through plastic deformation of the links, and the webs of the shear links exhibit stress traces. The specimens exhibit apparent local buckling phenomenon of the web plates, and the column base finally buckling under compression, leading to plastic deformation and specimen failure.

3.3 FE models and results

The finite element (FE) models were established in the SAP2000 software with version 15.2.1. In the FE models, the plastic hinges were defined at column-ends and beam-ends using the plastic hinges for steel column and beam in SAP2000 software based on the model presented in Tables

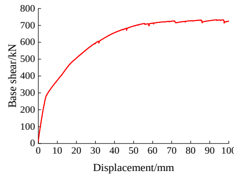

(a) Y-1 specimen

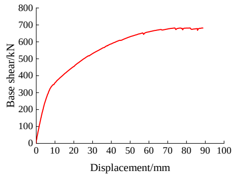

(b) Y-2 specimen

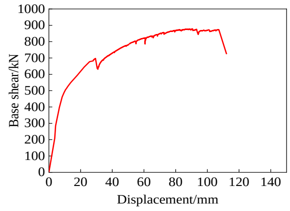

(c) K-type specimen

Fig. 9 Monotonic test curves

(a) Frame deformation

(b) Shear deformation of link

Fig. 10 Failure mode of K-type specimen

(a) Frame deformation

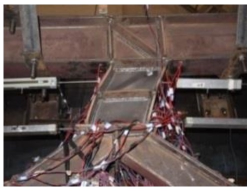

(b) Shear deformation of link

Fig. 11 Failure mode of Y-1 specimen

(a) Frame deformation

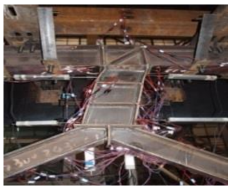

(b) Shear deformation of link

Fig. 12 Failure mode of Y-2 specimen

5-6 of FEMA-356 for steel column and beam. For the shear link, the model presented in Tables 5-6 of FEMA-356 was considered for the nonlinear behavior. The ultimate shear force of the shear link V_u=1.4V_p according to experimental results of shear links (Okazaki and Engelhardt 2015). Moreover, the immediate occupancy deformation □Δ_{IO}, life safety plastic deformation □Δ_{LS} and collapse prevention deformation □Δ_{CP} of the shear link were conducted using the parameters as suggested by Tables 5-6 of FEMA-356, as shown in Fig. 13

The hypotheses adopted for FE models was that, firstly, the approximate simplified element to simulate the members of the specimens, the members of the FE models are truss element; Secondly, the material property is

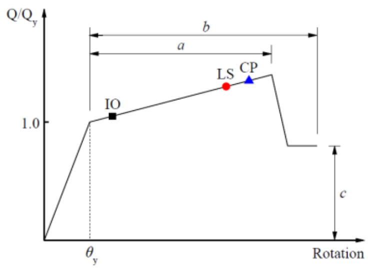

Fig. 13 Generalized force-deformation relation for shear link (FEMA-356)

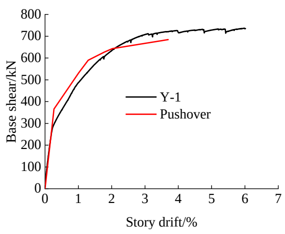

(a) Y-1

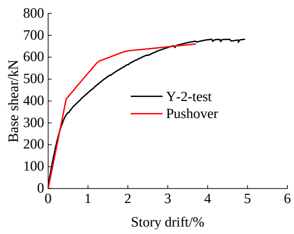

(b)Y-2

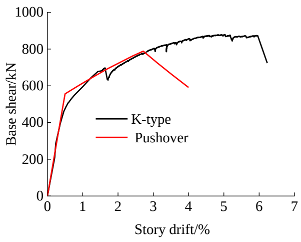

(c) K-type

Fig. 14 Comparison between analysis and test curves

approximated to the actual, the mean values of flange and web plate properties are used as the material properties of each component. Finally, the plastic deformation is isolated to the hinges, and the plastic hinges are rigid-plastic behavior. These hypotheses increase the uncertainty of the FE models (D. Gino *et al*. 2017).

The pushover curves obtained from the pushover analysis of the FE models are compared with the test monotonic loading curves in Fig.14. When the frame drift is more significant than H/50 (H is the height of the structure), the deformation of the link reaches the plastic limit state (AISC341-10). The failure mode of FE models from the pushover analysis is shown in Fig. 15.

The failure mode of FE models is similar with the monotonic tests (Fig. 16). The plastic deformations are mainly concentrated in the links, finally, the column base produces plastic deformation and the structure reaches the limit state. When the shear hinges with a rigid-plastic property unloading, and the pushover curves present a downward trend. The truss elements were used in FE models, and the mean value material properties of the flanges and web plates were taken as the material model. The plastic deformation of the structure was concentrated in the plastic hinges, as a result the plastic reaction of the structure is determined by the behavior of the plastic hinge. The plastic hinges of the structure reach the limit state in the FE models, unloading of the hinges occur, causing the bearing capacity to rapidly decrease. This is the primary

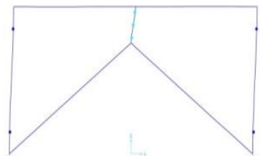

(a) Y-1

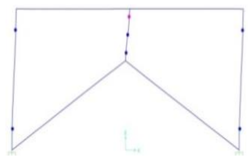

(b) Y-2

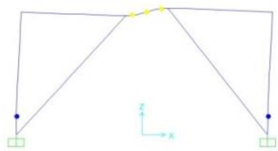

(c) K-type

Fig. 15 Failure mode of FE model

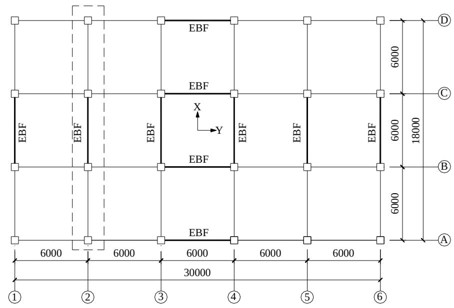

Fig. 16 The layout of prototype

cause errors between the results of FE models and the tests.

4. Finite element models of four types HSS-EBFs

In the finite element models of HSS-EBFs, Q345 steel used for the links and braces and Q460 steel utilized for the columns and beams. The elastic modulus of material is 2.06×10^5 MPa and the poisson's ratio is 0.3. There are four groups of design FE models, namely, 4-storey, 8-storey, 12-storey and 16-storey with the story height of 3.0 m. The FE models are characterized by a peak ground acceleration of 0.3 g with a 10% probability of exceedance over a 50-year period, and moderately firm ground conditions. The factor that reduces the elastic response spectrum to obtain the design spectrum is 2.8125 in GB50011-2010 (Code for seismic design of buildings in Chinese). The alpha damping, α, and beta damping, β, were specified according to the damping, ζ, and the fundamental period of the structures. In addition, damping of 4% is considered appropriate for a steel building with a structural height not exceeding 50 m, and 3% for structural heights between 50 - 200 m according to the requirements of GB50011-2010. In all design FE models, the concrete floor slab is 120 mm thick, and cast-in-place. The constraints between the columns of different stories were continuous, and rigid connections were used between columns and beams in all design examples. Box sections were used for the frame columns, and welded H-sections for the other members. The dead load on the floor was 5.0 kN/m^2, that including the floor weight, the floor live load was 2.0 kN/m^2, the roof dead load was 6.0 kN/m^2, the roof live load was 2.0 kN/m^2, the snow load was 0.35 kN/m^2, and the basic wind pressure was 0.35 kN/m^2.

Table 3 Member sections of D-type with S4

Story	Beam	Link	Column	Brace	$\rho=eV_p/M_p$
4	H300×100×6×10	H280×120×3×8	B250×250×12	H250×250×10×16	1.17
3	H300×150×8×12	H280×130×5×10	B250×250×12	H250×250×10×16	1.39
2	H300×150×10×16	H300×150×6×10	B250×250×12	H250×250×10×16	1.41
1	H330×150×10×16	H320×150×6×10	B250×250×12	H250×250×10×16	1.39

Table 4 Member sections of K-type with S4

Story	Beam	Link	Column	Brace	$\rho=eV_p/M_p$
4	H280×100×6×10	H340×120×4×10	B200×200×8	H160×160×8×12	1.19
3	H330×150×6×10	H300×150×8×12	B200×200×8	H180×180×8×12	1.53
2	H340×150×8×12	H310×150×10×16	B250×250×10	H200×200×8×12	1.44
1	H370×150×8×12	H340×150×10×16	B270×270×10	H200×200×8×12	1.41

Table 5 Member sections of V-type with S4

Story	Beam	Link	Column	Brace	$\rho=eV_p/M_p$
4	H350×100×6×10	H280×120×4×10	B280×280×10	H180×180×8×12	1.23
3	H360×150×8×12	H300×150×6×10	B300×300×10	H200×200×8×12	1.41
2	H360×150×10×16	H370×130×6×10	B320×320×12	H220×220×8×12	1.50
1	H400×150×10×16	H400×130×6×10	B340×340×12	H220×220×8×12	1.46

Table 6 Member sections of Y-type with S4

Story	Beam	Link	Column	Brace	$\rho=eV_p/M_p$
4	H300×100×4×8	H320×150×6×10	B250×250×10	H220×220×8×12	1.39
3	H300×140×6×10	H320×150×10×16	B280×280×10	H220×220×8×12	1.43
2	H320×160×6×10	H340×150×12×18	B300×300×12	H250×250×10×16	1.48
1	H350×160×6×10	H370×150×12×18	B300×300×12	H250×250×10×16	1.45

Table 7 Member sections of D-type with S8

Story	Beam	Link	Column	Brace	$\rho=eV_p/M_p$
8	H300×120×6×10	H250×130×4×8	B300×300×12	H220×220×10×16	1.42
7	H300×130×10×16	H300×150×6×10	B350×350×16	H220×220×10×16	1.41
6	H340×150×10×16	H350×150×6×10	B400×400×16	H250×250×10×16	1.36
5	H380×160×10×16	H400×150×6×10	B400×400×16	H250×250×10×16	1.32
4	H390×180×10×16	H350×150×8×12	B450×450×20	H250×250×10×16	1.47
3	H410×180×10×16	H380×150×8×12	B450×450×20	H250×250×10×16	1.44
2	H400×200×10×16	H400×150×8×12	B500×500×20	H250×250×10×16	1.42
1	H410×200×10×16	H410×150×8×12	B500×500×20	H250×250×10×16	1.41

Table 8 Member sections of K-type with S8

Story	Beam	Link	Column	Brace	$\rho=eV_p/M_p$
8	H300×120×6×10	H300×130×5×10	B280×280×12	H220×220×12×18	1.37
7	H320×150×8×12	H400×130×6×10	B280×280×12	H220×220×12×18	1.46
6	H330×150×10×16	H400×150×8×12	B320×320×16	H250×250×12×18	1.42
5	H370×150×10×16	H380×180×10×16	B320×320×16	H250×250×12×18	1.20
4	H400×150×10×16	H420×180×10×16	B350×350×16	H280×280×12×18	1.17
3	H410×160×10×16	H390×180×12×18	B350×350×16	H280×280×12×18	1.25
2	H400×180×10×16	H410×200×12×18	B380×380×16	H280×280×12×18	1.14
1	H410×180×10×16	H420×200×12×18	B380×380×16	H280×280×12×18	1.13

The plan layout of the FE models is shown in Fig. 16. There are five bays in the X-direction for one-bay EBF and three bays in the Y-direction for one-bay EBF, the spans in both the X- and Y-directions are 6.0 m. The length of the link is 800 mm.

The member sections of HSS-EBFs with four different forms are designed by PBSD method, as shown in Table 3-Table 18. In the tables, the length ratio of links is $\rho=eV_p/M_p$, and the links are shear yielding (or short link) when ρ is less than 1.6.

Table 9 Member sections of V-type with S8

Story	Beam	Link	Column	Brace	$\rho=eV_p/M_p$
8	H350×100×6×10	H300×150×5×8	B250×250×10	H180×180×8×12	1.46
7	H360×150×8×12	H300×150×6×10	B280×280×10	H200×200×8×12	1.41
6	H370×150×10×16	H380×130×6×10	B300×300×12	H220×220×8×12	1.48
5	H420×150×10×16	H450×130×6×10	B350×350×16	H220×220×8×12	1.41
4	H420×180×10×16	H400×150×8×12	B400×400×16	H220×220×8×12	1.42
3	H420×200×10×16	H420×150×8×12	B400×400×16	H250×250×10×16	1.40
2	H430×200×10×16	H440×150×8×12	B450×450×20	H250×250×10×16	1.38
1	H440×200×10×16	H450×150×8×12	B450×450×20	H250×250×10×16	1.37

hinges

Table 10 Member sections of Y-type with S8

Story	Beam	Link	Column	Brace	$\rho=eV_p/M_p$
8	H270×100×6×8	H320×120×6×12	B380×380×12	H220×220×10×16	1.43
7	H300×100×8×12	H320×150×10×16	B400×400×12	H240×240×10×16	1.43
6	H300×140×8×12	H350×150×12×18	B420×420×16	H250×250×12×18	1.47
5	H330×150×8×12	H410×200×12×18	B420×420×16	H250×250×12×18	1.14
4	H350×160×8×12	H400×200×14×20	B460×460×16	H280×280×12×18	1.18
3	H370×160×8×12	H430×200×14×20	B460×460×16	H280×280×12×18	1.17
2	H360×180×8×12	H450×200×14×20	B480×480×18	H280×280×12×18	1.15
1	H370×180×8×12	H460×200×14×20	B480×480×18	H280×280×12×18	1.15

Table 11 Member sections of D-type with S12

Story	Beam	Link	Column	Brace	$\rho=eV_p/M_p$
12	H300×120×6×10	H270×130×4×8	B300×300×12	H220×220×10×16	1.40
11	H340×150×8×12	H280×140×6×10	B400×400×16	H220×220×10×16	1.51
10	H420×150×8×12	H350×130×6×10	B450×450×16	H250×250×10×16	1.52
9	H400×150×10×16	H320×150×8×12	B450×450×16	H250×250×10×16	1.51
8	H440×150×10×16	H360×150×8×12	B500×500×20	H280×280×10×16	1.46
7	H400×200×10×16	H330×150×10×16	B500×500×20	H280×280×10×16	1.42
6	H430×200×10×16	H350×150×10×16	B550×550×20	H300×300×14×20	1.40
5	H400×200×12×18	H370×150×10×16	B550×550×20	H300×300×14×20	1.38
4	H420×200×12×18	H390×150×10×16	B600×600×25	H300×300×14×20	1.36
3	H430×200×12×18	H400×150×10×16	B600×600×25	H300×300×14×20	1.36
2	H440×200×12×18	H410×150×10×16	B650×650×25	H300×300×14×20	1.35
1	H440×200×12×18	H410×150×10×16	B650×650×25	H300×300×14×20	1.35

Table 12 Member sections of K-type with S12

Story	Beam	Link	Column	Brace	$\rho=eV_p/M_p$
12	H300×120×6×10	H300×150×5×10	B200×200×10	H200×200×10×16	1.22
11	H330×150×8×12	H310×150×8×12	B250×250×10	H200×200×10×16	1.52
10	H330×150×10×16	H320×150×10×16	B250×250×12	H250×250×10×16	1.43
9	H380×150×10×16	H380×150×10×16	B250×250×12	H250×250×10×16	1.37
8	H420×150×10×16	H430×200×10×16	B300×300×12	H250×250×10×16	1.07
7	H400×180×10×16	H400×200×12×18	B300×300×12	H250×250×10×16	1.14
6	H430×180×10×16	H430×200×12×18	B300×300×16	H280×280×12×18	1.13
5	H450×180×10×16	H450×200×12×18	B350×350×18	H280×280×12×18	1.11
4	H430×200×10×16	H470×200×12×18	B400×400×20	H280×280×12×18	1.10
3	H440×200×10×16	H480×200×12×18	B450×450×20	H280×280×12×18	1.10
2	H450×200×10×16	H490×200×12×18	B500×500×20	H280×280×12×18	1.09
1	H450×200×10×16	H500×200×12×18	B500×500×20	H280×280×12×18	1.09

In this paper, the SAP2000 finite element software is used to analyze the seismic performance of HSS-EBFs. Shear plastic hinges (V2 hinge) are arranged in the middle and both ends of the links, flexural plastic hinges (M3 hinge) are set in frame beams, compression-bending related hinges (P-M3 hinge) are set in columns, and axial force (hinge P) are set in braces. The material parameters are nominal value and the elastic modulus $E=2.06\times10^5$ MPa. The representative value of gravity load on the standard floor is 930.5 kN and that on the top layer is 807 kN. The first three periods of the structure are obtained by modal analysis of structures, as seen in Table 19. According to the

Table 13 Member sections of V-type with S12

Story	Beam	Link	Column	Brace	$\rho=eV_p/M_p$
12	H360×100×6×10	H300×130×5×10	B250×250×10	H220×220×8×12	1.37
11	H360×150×8×12	H300×150×6×10	B300×300×12	H220×220×8×12	1.41
10	H370×150×10×16	H380×150×6×10	B350×350×16	H220×220×8×12	1.34
9	H430×150×10×16	H450×130×6×10	B350×350×16	H220×220×8×12	1.41
8	H440×170×10×16	H400×150×8×12	B400×400×16	H250×250×10×16	1.42
7	H430×200×10×16	H430×150×8×12	B400×400×16	H250×250×10×16	1.39
6	H460×200×10×16	H460×150×8×12	B450×450×20	H250×250×10×16	1.36
5	H480×200×10×16	H410×200×10×16	B450×450×20	H250×250×10×16	1.08
4	H500×200×10×16	H430×200×10×16	B500×500×20	H250×250×10×16	1.07
3	H510×200×10×16	H440×200×10×16	B500×500×20	H280×280×12×18	1.07
2	H520×200×10×16	H450×200×10×16	B550×550×25	H280×280×12×18	1.06
1	H530×200×10×16	H460×200×10×16	B550×550×25	H280×280×12×18	1.06

Table 14 Member sections of Y-type with S12

Story	Beam	Link	Column	Brace	$\rho=eV_p/M_p$
12	H300×100×4×8	H320×150×6×10	B360×360×16	H280×280×12×18	1.39
11	H350×100×6×10	H390×150×8×12	B360×360×16	H280×280×12×18	1.43
10	H350×150×6×10	H420×150×10×16	B400×400×20	H300×300×14×20	1.34
9	H340×150×8×12	H490×200×10×16	B400×400×20	H300×300×14×20	1.04
8	H380×150×8×12	H470×200×12×18	B450×450×20	H350×350×14×20	1.10
7	H410×150×8×12	H520×200×12×18	B450×450×20	H350×350×14×20	1.07
6	H360×150×10×16	H560×200×12×18	B500×500×20	H350×350×14×20	1.05
5	H380×150×10×16	H590×200×12×18	B500×500×22	H400×400×14×20	1.04
4	H390×150×10×16	H540×200×14×20	B550×550×22	H400×400×14×20	1.10
3	H400×150×10×16	H560×200×14×20	B550×550×22	H400×400×14×20	1.09
2	H400×150×10×16	H570×200×14×20	B600×600×25	H400×400×14×20	1.08
1	H410×150×10×16	H580×200×14×20	B600×600×25	H400×400×14×20	1.08

Table 15 Member sections of D-type with S16

Story	Beam	Link	Column	Brace	$\rho=eV_p/M_p$
16	H300×130×6×10	H250×130×4×8	B250×250×12	H250×250×10×16	1.42
15	H410×140×6×10	H320×150×5×10	B300×300×12	H250×250×10×16	1.21
14	H410×200×6×10	H350×150×6×10	B350×350×12	H280×280×12×18	1.36
13	H410×200×8×12	H320×150×8×12	B350×350×16	H280×280×12×18	1.51
12	H450×200×8×12	H360×150×8×12	B450×450×16	H280×280×12×18	1.46
11	H400×200×10×16	H330×150×10×16	B450×450×16	H280×280×12×18	1.42
10	H430×200×10×16	H360×150×10×16	B500×500×20	H300×300×14×20	1.39
9	H410×200×12×18	H380×150×10×16	B500×500×20	H300×300×14×20	1.37
8	H430×200×12×18	H400×200×10×16	B550×550×20	H300×300×14×20	1.09
7	H440×200×12×18	H410×200×10×16	B550×550×20	H300×300×14×20	1.08
6	H450×200×12×18	H430×200×10×16	B600×600×25	H300×300×14×20	1.07
5	H460×200×12×18	H440×200×10×16	B600×600×25	H300×300×14×20	1.07
4	H470×200×12×18	H450×200×10×16	B650×650×25	H350×350×14×20	1.06
3	H480×200×12×18	H460×200×10×16	B650×650×25	H350×350×14×20	1.06
2	H480×200×12×18	H460×200×10×16	B750×750×30	H350×350×14×20	1.06
1	H490×200×12×18	H470×200×10×16	B750×750×30	H350×350×14×20	1.05

fundamental period of the structure, the fundamental period of D-type HSS-EBFs is the minimum, and that of Y-type HSS-EBFs is the maximum, which indicates that the lateral stiffness of D-type HSS-EBFs is the largest and that of Y-type HSS-EBFs is the weakest.

5. Pushover analysis

5.1 Capacity curves

The analysis models of the structures are established by SAP2000. The links yield in a shear mode, meanwhile, all of the cross sections along the length of the links yield simultaneously. Therefore, shear hinges are designated at both ends and middle of the links, and three shear hinges yield at the same time. Horizontal loading adopt the inverted triangular distribution mode, pushing the structure

Table 16 Member sections of K-type with S16

Story	Beam	Link	Column	Brace	$\rho=eV_p/M_p$
16	H300×120×6×10	H300×150×5×10	B200×200×10	H180×180×10×16	1.22
15	H330×150×8×12	H300×150×8×12	B250×250×12	H180×180×10×16	1.53
14	H330×150×10×16	H320×150×10×16	B250×250×12	H200×200×10×16	1.43
13	H380×150×10×16	H380×150×10×16	B250×250×12	H200×200×10×16	1.37
12	H420×150×10×16	H420×200×10×16	B300×300×16	H220×220×10×16	1.08
11	H410×180×10×16	H400×200×12×18	B300×300×16	H220×220×10×16	1.14
10	H430×180×10×16	H430×200×12×18	B350×350×16	H250×250×10×16	1.13
9	H450×180×10×16	H450×200×12×18	B400×400×16	H250×250×10×16	1.11
8	H450×200×10×16	H470×200×12×18	B420×420×16	H250×250×10×16	1.10
7	H460×200×10×16	H490×200×12×18	B450×450×20	H280×280×12×18	1.09
6	H470×200×10×16	H510×200×12×18	B500×500×20	H280×280×12×18	1.08
5	H480×200×10×16	H520×200×12×18	B500×500×20	H280×280×12×18	1.07
4	H490×200×10×16	H540×200×12×18	B550×550×20	H280×280×12×18	1.06
3	H500×200×10×16	H540×200×12×18	B580×580×25	H280×280×12×18	1.06
2	H500×200×10×16	H550×200×12×18	B650×650×25	H280×280×12×18	1.06
1	H500×200×10×16	H550×200×12×18	B650×650×25	H280×280×12×18	1.06

Table 17 Member sections of V-type with S16

Story	Beam	Link	Column	Brace	$\rho=eV_p/M_p$
16	H320×100×8×12	H300×130×5×10	B250×250×12	H250×250×10×16	1.37
15	H370×150×8×12	H300×150×6×10	B250×250×12	H250×250×10×16	1.41
14	H380×150×10×16	H380×150×6×10	B300×300×16	H250×250×10×16	1.34
13	H430×150×10×16	H460×130×6×10	B300×300×16	H250×250×10×16	1.40
12	H400×200×10×16	H400×150×8×12	B350×350×16	H280×280×12×18	1.42
11	H440×200×10×16	H440×150×8×12	B350×350×16	H280×280×12×18	1.38
10	H470×200×10×16	H390×150×10×16	B400×400×16	H280×280×12×18	1.36
9	H490×200×10×16	H420×200×10×16	B400×400×16	H300×300×14×20	1.08
8	H470×200×12×18	H440×200×10×16	B450×450×20	H300×300×14×20	1.07
7	H490×200×12×18	H460×200×10×16	B450×450×20	H300×300×14×20	1.06
6	H500×200×12×18	H410×200×12×18	B500×500×22	H300×300×14×20	1.14
5	H510×200×12×18	H420×200×12×18	B500×500×22	H300×300×14×20	1.13
4	H520×200×12×18	H430×200×12×18	B550×550×25	H300×300×14×20	1.13
3	H530×200×12×18	H440×200×12×18	B550×550×25	H300×300×14×20	1.12
2	H540×200×12×18	H450×200×12×18	B600×600×28	H300×300×14×20	1.11
1	H540×200×12×18	H460×200×12×18	B600×600×28	H300×300×14×20	1.11

Table 18 Member sections of Y-type with S16

Story	Beam	Link	Column	Brace	$\rho=eV_p/M_p$
16	H310×100×5×8	H330×150×6×10	B350×350×16	H300×300×12×18	1.38
15	H360×100×6×10	H340×200×10×16	B350×350×16	H300×300×12×18	1.12
14	H310×150×8×12	H430×200×10×16	B400×400×20	H300×300×14×20	1.07
13	H350×150×8×12	H430×200×12×18	B400×400×20	H300×300×14×20	1.13
12	H390×150×8×12	H430×200×14×20	B450×450×20	H350×350×14×20	1.17
11	H420×150×8×12	H470×200×14×20	B450×450×20	H350×350×14×20	1.14
10	H370×150×10×16	H510×200×14×20	B500×500×22	H400×400×14×20	1.12
9	H390×150×10×16	H540×200×14×20	B500×500×22	H400×400×14×20	1.10
8	H410×150×10×16	H570×200×14×20	B550×550×25	H400×400×14×20	1.08
7	H410×160×10×16	H600×200×14×20	B550×550×25	H400×400×14×20	1.06
6	H420×160×10×16	H620×200×14×20	B600×600×25	H450×450×14×20	1.05
5	H400×180×10×16	H640×200×14×20	B600×600×25	H450×450×14×20	1.04
4	H410×180×10×16	H660×200×14×20	B650×650×25	H450×450×14×20	1.03
3	H420×180×10×16	H670×200×14×20	B650×650×25	H450×450×14×20	1.03
2	H430×180×10×16	H680×200×14×20	B700×700×28	H450×450×14×20	1.02
1	H430×180×10×16	H690×200×14×20	B700×700×28	H450×450×14×20	1.02

to the ultimate state. The structural model is pushed to the maximum plastic hinge deformation, with the ultimate state of the structure. The loading capacity at this time is called the ultimate bearing capacity. The capacity curves of the

Table 19 The fundamental period

Examples	T_1/s	T_2/s	T_3/s
K-4	0.578	0.210	0.134
K-8	0.816	0.289	0.166
K-12	1.264	0.439	0.239
K-16	1.659	0.562	0.305
Y-4	0.724	0.275	0.166
Y-8	0.125	0.409	0.232
Y-12	1.490	0.528	0.304
Y-16	1.891	0.649	0.368
D-4	0.458	0.177	0.127
D-8	0.717	0.249	0.148
D-12	0.999	0.339	0.192
D-16	1.351	0.445	0.244
V-4	0.546	0.202	0.131
V-8	0.929	0.326	0.192
V-12	1.273	0.429	0.244
V-16	1.696	0.563	0.306

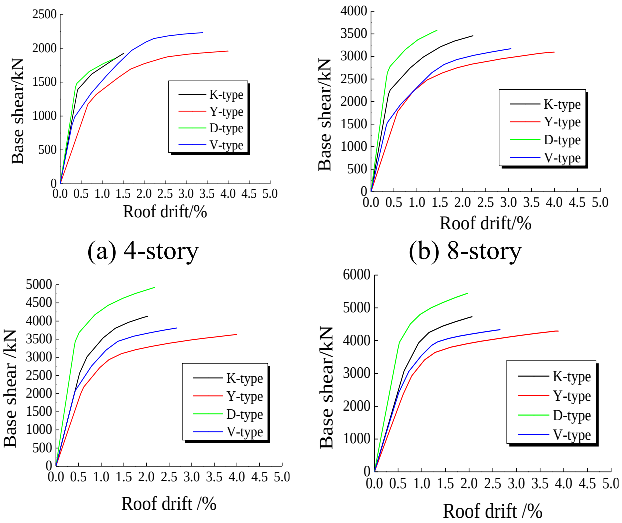

(a) 4-story (b) 8-story

(c) 12-story (d) 16-story

Fig. 17 Pushover curves

base shear force and the roof drift of the structure are obtained, as shown in Fig. 17. From the capacity curves, the lateral stiffness of D-type HSS-EBF structure is the largest. With the increase of the total height of the structure, the difference of structural stiffness becomes more and more obvious, while the lateral stiffness of Y-type EBF is the smallest. Because the lateral stiffness of the structure is mainly provided by braces, and the brace angle determines the lateral stiffness of the structure, among which the brace angle of D-type EBF is the largest, whereas the brace angle of Y-type EBF is the smallest. However, the ductility of Y-type HSS-EBF structure is the best, and the roof drift of the frame has reached more than 4% in the ultimate state. Y-type eccentrically braced structure is different from the other three forms and its links are independent of the frame beams, after the links entered the plastic state, the structural response is similar to moment-resisting frames structure, and the frame beams continue to dissipate energy by the flexural plastic deformation, and the structural ductility is closed to steel frame structure.

5.2 Ultimate state of HSS-EBFs

Figs. 18, 19, 20, and 21 show the plastic hinges distribution of HSS-EBFs structure when it is pushed to the ultimate state. From the development of plastic hinges and ultimate failure mode, it can be seen that the links enter the elastic-plastic state first, and nearly links yielding at each story. Then the frame beam acts as the second seismic resist member. When the plastic development of links reaches a certain condition, the links begin to dissipate energy by flexural yielding. Finally, the column bases reach to the plastic state, which meets multi-defenses criterion in seismic design. When the structure is pushed to the ultimate state, the links participate in energy dissipation. The story drifts and link rotations are distributed evenly along the height of the structure, and no weak layers arise. Finally, the column base is damaged by forming plastic hinges and transforming into mechanism. The ultimate state of FE models is in accordance with the predicted failure mode based on performance-based seismic design, which is close to the expected overall failure target.

6. Time history analysis

6.1 Ground motion selection

The seismic ground motions consist of 10 actual and 1 artificial records. Table 20 show the seismic ground motions of each actual records, including the location and time of the earthquake event, the recording station, magnitude *M*, the near-fault distances *R*, the peak ground acceleration *PGA* (g) and the peak ground velocity *PGV* (cm/s). The spectrum characteristics, duration, maximum acceleration, recording points and pulse effects of each seismic record are different. By amplifying the peak acceleration of seismic records to three seismic hazard levels, first, elastic behavior in low earthquake hazard level for immediate occupancy (the corresponding peak ground acceleration is 110 cm/s^2), second, inelastic behavior of links in moderate earthquake hazard level for rapid repair (the corresponding peak ground acceleration is 300 cm/s^2), and third, the inelastic behavior of the whole structure in very high earthquake hazard level for collapse prevention (the corresponding peak ground acceleration is 510 cm/s^2).

The nonlinear dynamic analysis of the structure under different seismic levels is conducted by inputting several earthquake records in SAP2000, in which the mean values of structure deformation, i.e., story drifts and link rotations, under different earthquake records are selected.

The Code for Seismic Design of Buildings in China(GB50010-2010) stipulates that when using time history analysis method, the actual ground motion records and artificial acceleration records should be selected according to the site conditions. Among them, the number of actual strong ground motion records should not be less than 2/3 of the total number. The mean value of seismic influence coefficient of multi-group time history curves should be consistent with the seismic influence coefficient curve adopted by the mode-superposition response

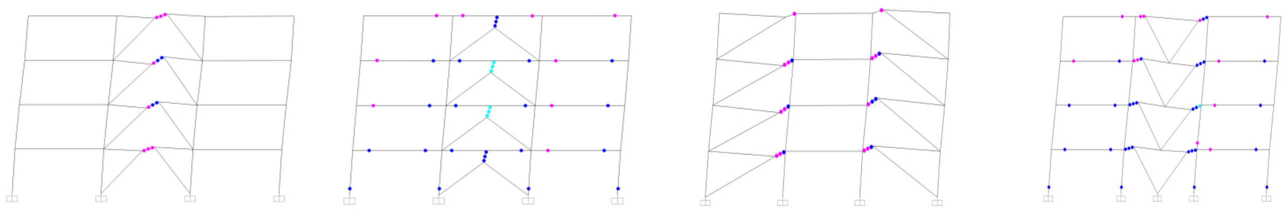

(a) K-type (b) Y-Type (c) D-type (d) V-type

Fig. 18 Failure mode of 4-story buildings

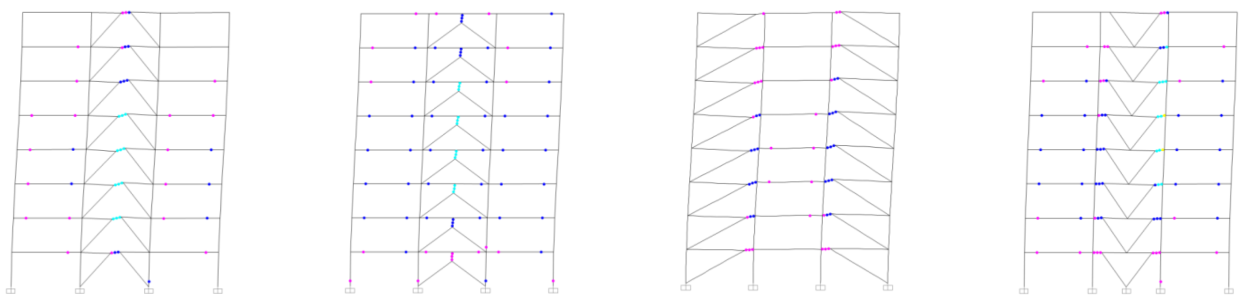

(a) K-type (b) Y-Type (c) D-type (d) V-type

Fig. 19 Failure mode of 8-story buildings

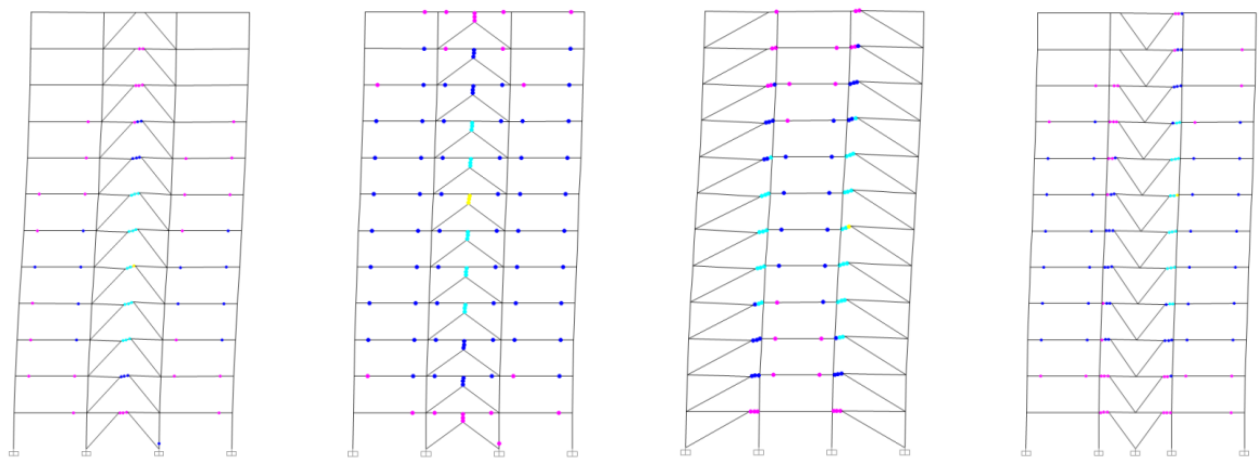

(a) K-type (b) Y-Type (c) D-type (d) V-type

Fig. 20 Failure mode of 12-story buildings

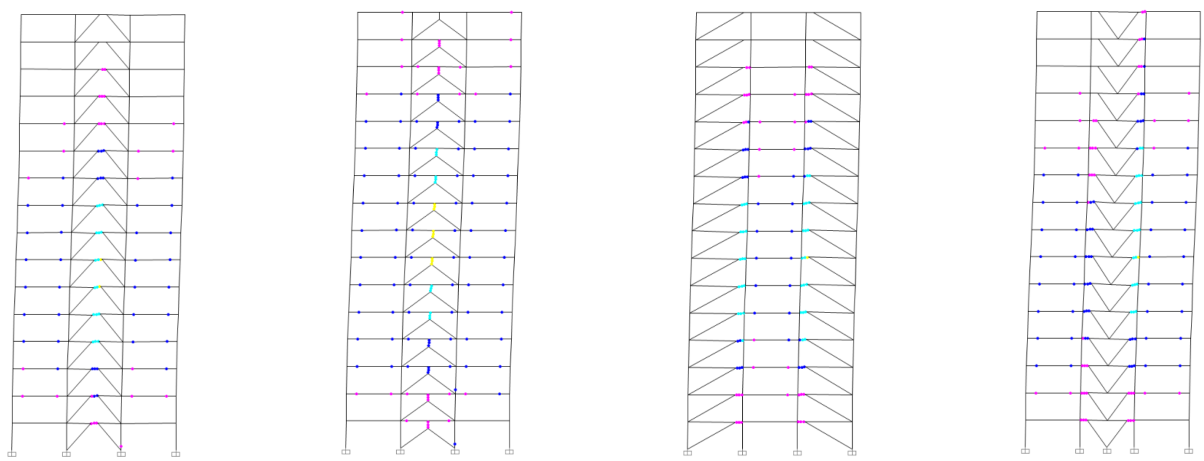

(a) K-type (b) Y-Type (c) D-type (d) V-type

Fig. 21 Failure mode of 16-story buildings

Table18 Ground motion records

No.	Earthquake number	Earthquake event	Station	M	R/km	PGA/g	PGV/(cm/s)
1	NGA0181	Imperial Valley 1979/10/15 23:16	942 El Centro Array #6	6.5	1.0	0.439	109.8
2	NGA0829	Cape Mendocino 1992/04/25 18:06	89324 Rio Dell Overpass - FF	7.0	14.3	0.549	42.1
3	NGA0292	Irpinia, Italy 1980/11/23 19:34	Sturno	6.5	3.2	0.358	52.7
4	NGA0727	Superstitn Hills(B) 1987/11/24 13:16	01335 El Centro Imp. Co. Cent	6.5	5.6	0.894	42.2
5	NGA0802	Loma Prieta 1989/10/18 00:05	58065 Saratoga - Aloha Ave	6.9	13.0	0.324	41.2
6	NGA0821	Erzincan, Turkey 1992/03/13	95 Erzincan	6.9	2.0	0.496	64.3
7	NGA1485	Chi-Chi, Taiwan 1999/09/20	TCU045	7.6	24.1	0.512	39.0
8	NGA0068	San Fernando 1971/02/09 14:00	135 LA - Hollywood Stor Lot	6.6	21.2	0.210	18.9
9	NGA0960	Northridge 1994/01/17 12:31	90057 Canyon Country - W Lost Cany	6.7	13.0	0.482	45.1
10	NGA1605	Duzce, Turkey 1999/11/12	Duzce	7.1	8.2	0.535	83.5

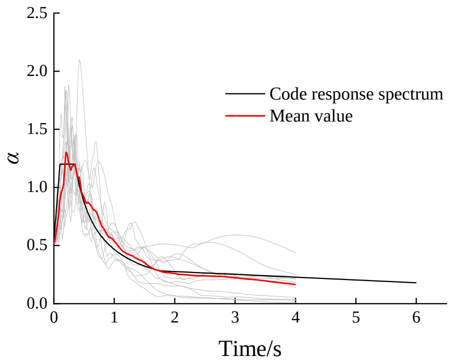

Fig. 22 Seismic response spectrum

spectrum method in statistical sense. It is means that the mean value of seismic influence coefficient of ground motion records are not more than 20% different from those of the seismic influence coefficient curves used in the mode-superposition response spectrum method at the periodic points corresponding to the main modes of the structure. Fig. 22 shows the comparison between the response spectrum mean value of seismic records and the response spectrum of the code. It can be seen that the response spectrum mean value coincide well with the code response spectrum at the periodic points of the main modes of the structure. The mean value of the time history analysis results can be used in the nonlinear dynamic analysis.

6.2 Failure mode

The failure modes of all FE models under rare earthquakes are shown in Fig. 23, and only the elastic-plastic state of structures under the excitation of NGA0068 seismic record is given in the limited space. The plastic deformation is isolated to all links in the structures. Almost each links dissipate energy by plastic deformation, and the plastic deformation of the links distributes evenly along the height, thus all failure modes are nearly to an expected condition. The other members, such as frame beams, columns and braces, are still in the elastic state, so it is not necessary to put forward excessive plastic deformation requirements for the materials of frame beams and columns. It is required that high strength steel can be used to effectively reduce the cross-section of components, while promoting high strength steel to be applied to seismic fortification structures. The links uses ordinary steel, which has excellent elastic-plastic deformation capacity to dissipate energy and protect the main structure in the elastic state. The story drifts distribution along the structure height is uniform. With the increase of the height, the structure gradually changes from shear failure to bend-shear failure, and the elastic-plastic deformation of links in the middle stories increases, and the plastic hinges of the middle links develop to a greater extent, while the top and bottom story consume less energy. As a whole, the failure mode of the structure has reached the expectation of performance-based seismic design.

6.3 Story drift and Link rotation

The mean values of story drift and link rotation of different types EBFs under 11 seismic records are shown in Figs. 24 - 29. The results indicated that the story drift under minor earthquakes (corresponding to the low earthquake hazard level for immediate occupancy) doesn't exceed the elastic limit value of 0.4% (H/250, H is the total height of the structure), and that the story drift under rare earthquakes (corresponding to the high earthquake hazard level for collapse prevention) does not exceed the plastic limit value of 2% (H/50). The elastic and plastic link rotation does not exceed the limit value of 0.02 rad and 0.08 rad (AISC341-10), respectively. Among them, Y-type eccentric brace has the largest story drift and link rotation, which is consistent with pushover analysis results. The stiffness of Y-type EBFs is the worst in the four types of eccentric brace, while the stiffness of D-type eccentric brace is the largest, and the story drift and link rotation are the minimum, for the D-type eccentric brace has the largest brace angle and the largest lateral stiffness. Except for the bottom story, the story drift of each structure is between 0.4% and 1.2%, which indicates that the distribution of story drift is basically uniform along the height, and accords with the expected failure mode. The lower story drift of first storey is due to the rigid connection of the column base and the larger stiffness of the bottom storey. The link rotation is between 0.01 and 0.03 rad, which shows that the links are basically involved in the elastic-plastic energy dissipation. The elastic-plastic deformation of the links distributes evenly along the height, and it is close to the expected overall failure mode.

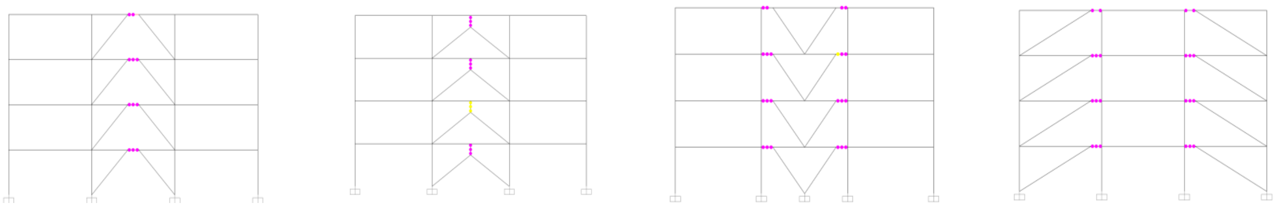

(a) 4-story

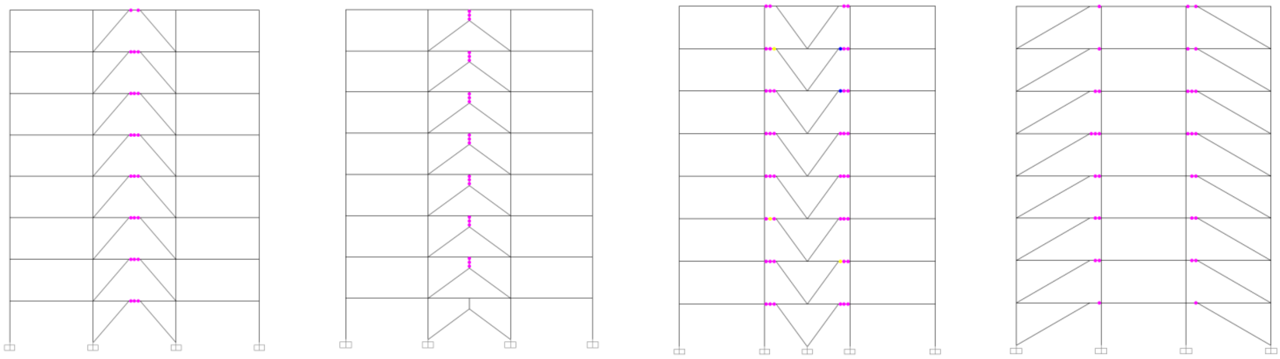

(b) 8-story

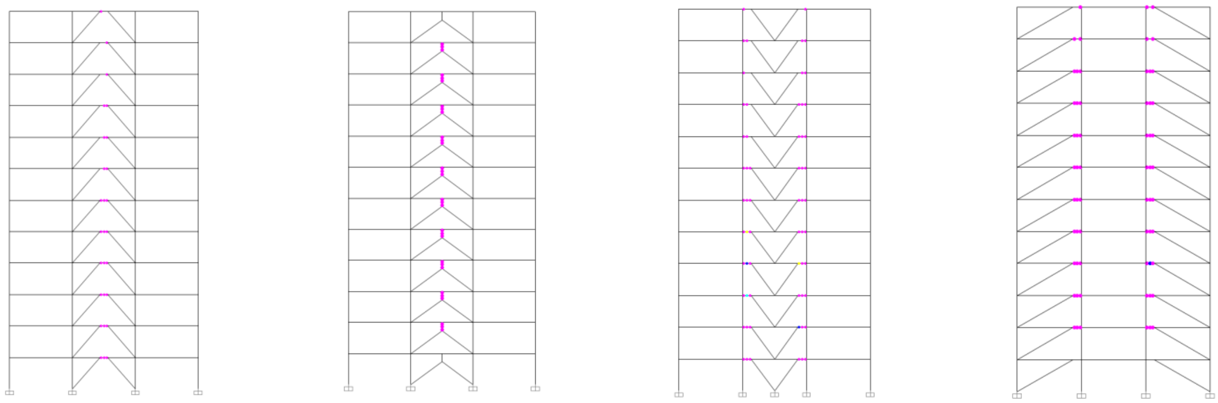

(c) 12-stroy

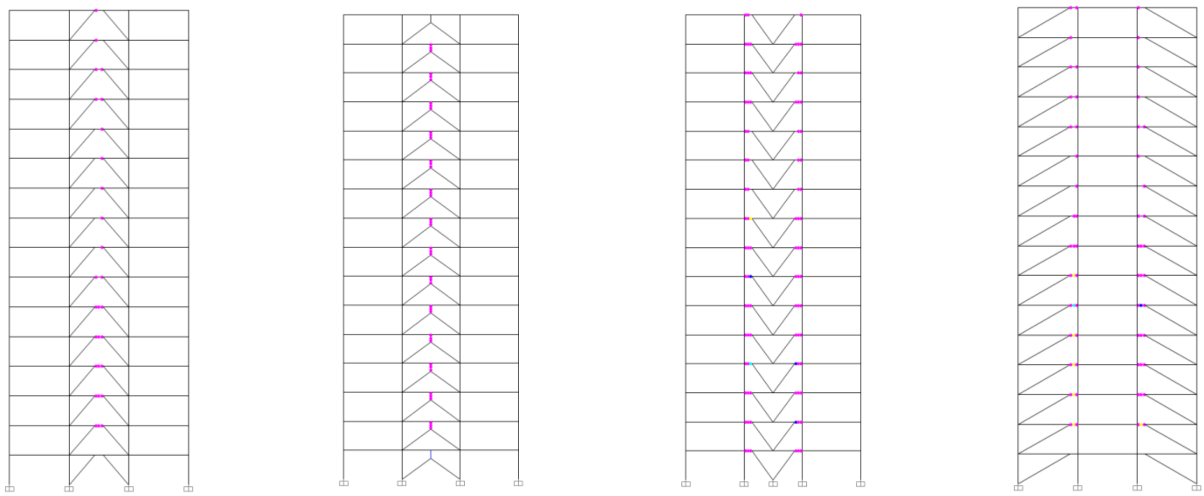

(d) 16-story

Fig. 23 Failure modes of all models under rare earthquakes

7. Conclusions

In this paper, four groups of D-type, K-type, Y- type and V-type HSS-EBFs are designed by performance-based seismic design method. The seismic performance of the structures is evaluated by pushover analysis and nonlinear dynamic analysis. The conclusions are as follows:

- The failure modes of four types of HSS-EBFs are in accord with the anticipated goal of performance-based seismic design method. Links are involved in energy

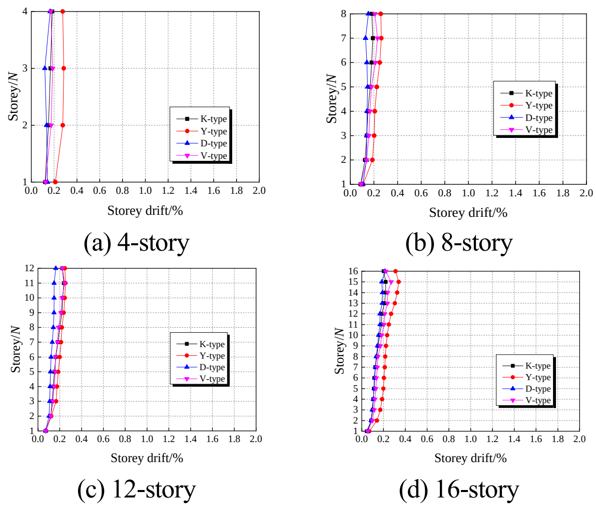

(a) 4-story (b) 8-story

(c) 12-story (d) 16-story

Fig. 24 The story drifts in IO seismic level

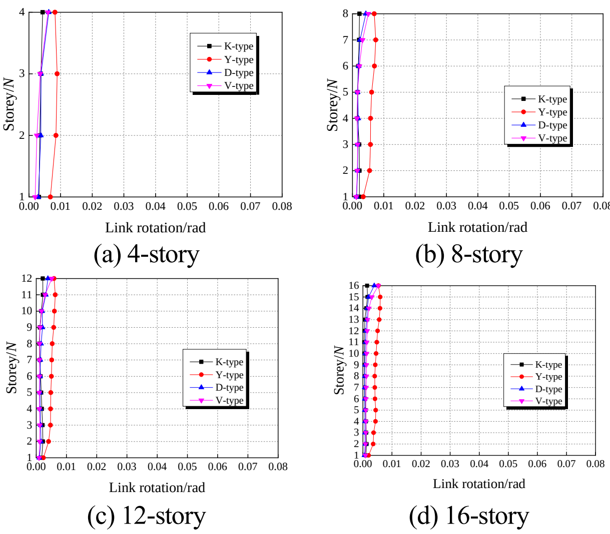

(a) 4-story (b) 8-story

(c) 12-story (d) 16-story

Fig. 25 The link rotations in IO seismic level

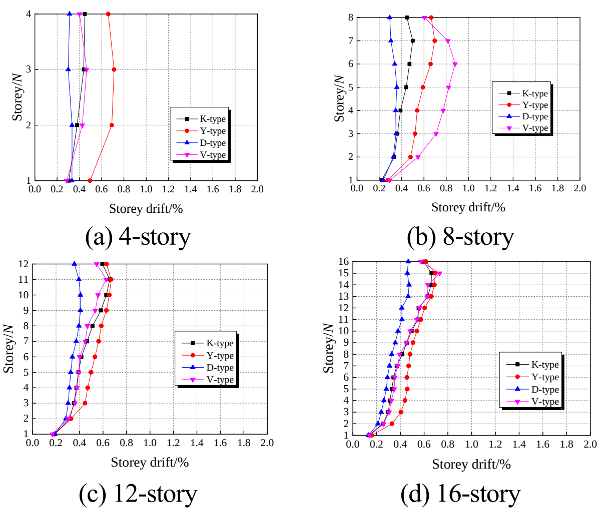

(a) 4-story (b) 8-story

(c) 12-story (d) 16-story

Fig. 26 The story drifts in RR seismic level

dissipation, story drift is evenly distributed along the height of the structure, and there are no weak layers.

• The lateral stiffness and bearing capacity of D-shaped

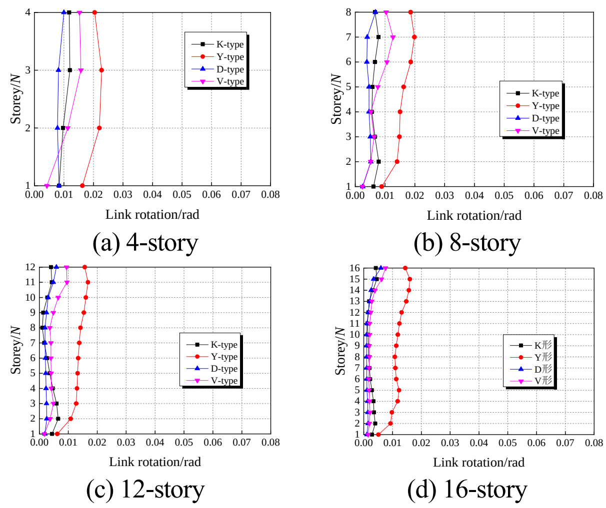

(a) 4-story (b) 8-story

(c) 12-story (d) 16-story

Fig. 27 The link rotations in RR seismic level

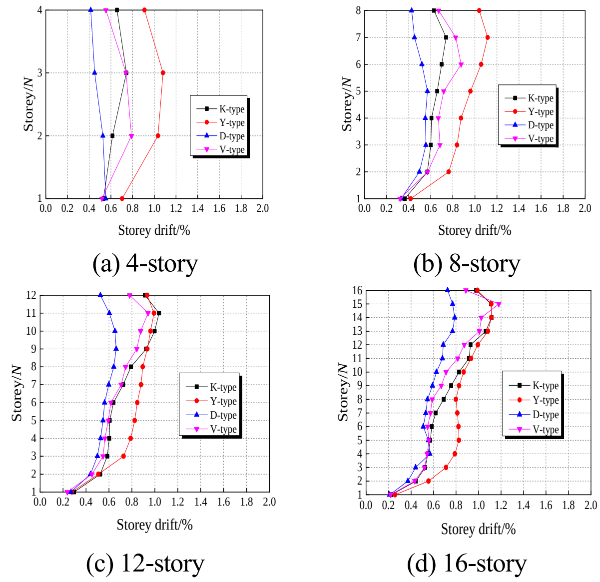

(a) 4-story (b) 8-story

(c) 12-story (d) 16-story

Fig. 28 The story drifts in CP seismic level

HSS-EBFs are the largest, while that of Y-shaped HSS-EBFs is the smallest, but Y-shaped HSS-EBFs have the best ductility.

• Under rare earthquakes, only links enter plastic deformation state to dissipate energy in all EBFs, and the elastic-plastic deformation of the links distributes evenly along the height of the structure. The remaining members are in the state of elasticity. The non-energy-dissipating members can effectively reduce the section of members by using high-strength steel, so as to promote the application of high-strength steel in the seismic fortification area.

• All EBFs under rare earthquakes have not exceeded the limit of the code in terms of story drift and link rotation, and the distribution of story drift and link rotation angle along the height are more uniform. Among them, the Y-shaped eccentrically braced structure has the largest story drift and link rotation, while the D-shaped eccentrically braced structure has the smallest story drift and link rotation.

Acknowledgments

The authors are grateful for the financial support received from the National Natural Science Foundation of China (Grant No. 51978571) and the Project Supported by Natural Science Basic Research Plan in Shaanxi Province of China (Program No. 2018JQ5056 and 2019JQ-727) and The Project Supported by Shaanxi Postdoctoral Science Foundation (No. 2018BSHEDZZ24).

References

AISC341-10 (2010), "Seismic Provision for Structure Steel Buildings", American Institute of Steel Construction, Chicago, U.S.A.

Azad, S.K. and Topkaya, C. (2017), "A review of research on steel eccentrically braced frames", J. *Construct. Steel Res.*, **128**(1), 53-73. https://doi.org/10.1016/j.jcsr.2016.07.032.

Ashtari, A. and Erfani, S. (2016), "An analytical model for shear links in eccentrically braced frames", *Steel Compos. Struct.*, **22**(3), 627-645. https://doi.org/10.12989/scs.2016.22.3.627.

Bosco, M. and Rossi, P.P. (2009), "Seismic behaviour of eccentrically braced frames", *Eng. Struct.*, **31**(3), 664-674. https://doi.org/10.1016/j.engstruct.2008.11.002.

Caprili, S., Mussini, N. and Salvatore, W. (2018), "Experimental and numerical assessment of EBF structures with shear links", *Steel Compos. Struct.*, **28**(2), 123-128. https://doi.org/10.12989/scs.2018.28.2.123.

Castaldo, P., Amendola, G. and Palazzo, B. (2016), "Seismic fragility and reliability of structures isolated by friction pendulum devices: seismic reliability-based design (SRBD)", *Earthq. Eng. Struct. Dyn.*, **46**(3), 425-446. https://doi.org/10.1002/eqe.2798.

CSI (2012), "Integrated software for structural analysis and design, SAP2000 version 15.2.1", Computer and Structures, Inc., California, U.S.A.

Di, Trapani, F., Bertagnoli, G., Ferrotto, M.F. and Gino, D. (2018), "Empirical equations for the direct definition of stress-strain laws for fiber-section-based macromodeling of infilled frames", *J. Eng. Mech.*, **144**(11), 04018101. https://doi.org/10.1061/(ASCE)EM.1943-7889.0001532.

Gino, D., Bertagnoli, G., La Mazza, D. and Mancini, G. (2017), "A quantification of model uncertainties in NLFEA of R.C. shear walls subjected to repeated loading", *Int. J. Earthq. Eng.*, **34**(3), 79-91.

Dubina, D., Stratan, A. and Dinu, F. (2010), "Dual high-strength steel eccentrically braced frames with removable links", *Earthq. Eng. Struct. Dyn.*, **37**(15), 1703-1720. https://doi.org/10.1002/eqe.828.

FEMA356 (2000), "Seismic Rehabilitation of Buildings", Federal Emergency Management Agency, Washington D.C., U.S.A.

GB50011-2010 (2010), "Code for seismic design of buildings", China Architecture Industry Press, Beijing, China.

Li, S., Tian, J.B. and Liu, Y.H. (2017). "Performance-based seismic design of eccentrically braced steel frames using target drift and failure mode", *Earthq. Struct.*, **13**(5), 443-454. https://doi.org/10.12989/eas.2017.13.5.443.

Li, S., Wang, C.Y., Li, X.L., Jian, Z. and Tian, J.B. (2018), "Seismic behavior of K-type eccentrically braced frames with high strength steel based on PBSD method", *Earthq. Struct.*, **15**(6), 667-684. https://doi.org/10.12989/eas.2018.15.6.667.

Li, S., Liu, Y.H. and Tian, J.B. (2018), "Experimental and analytical study of eccentrically braced frames combined with high-strength steel", *Int. J. Steel Struct.*, **18**(2), 528-533. https://doi.org/10.1007/s13296-018-0018-x.

Li, S., Tian J.B. and Liu Y.H. (2017), "Performance-based seismic design of eccentrically braced steel frames using target drift and failure mode", *Earthq. Struct.*, **13**(5), 443-454. https://doi.org/10.12989/eas.2017.13.5.443.

Lian, M., Su, M.Z. and Guo, Y. (2015), "Seismic performance of eccentrically braced frames with high strength steel combination", *Steel Compos. Struct.*, **18**(6), 1517-1539. https://doi.org/10.12989/scs.2015.18.6.1517.

Lian, M. and Su, M.Z. (2017), "Seismic performance of high-strength steel fabricated eccentrically braced frame with vertical shear link", *J. Construct. Steel Res.*, **137**(10), 262-285.

Lian, M., and Su, M. Z. (2017), "Experimental study and simplified analysis of ebf fabricated with high strength steel", *Journal of Constructional Steel Research*, **139**(12), 6-17. https://doi.org/10.1016/j.jcsr.2017.06.022.

Mohammadi, R.K. and Sharghi, A.H. (2014), "On the optimum performance-based design of eccentrically braced frames". *Steel Compos. Struct.*, **16**(4), 357-374. http://dx.doi.org/10.12989/scs.2014.16.4.357.

Okazaki, T. and Engelhardt, M.D. (2015), "Cyclic loading behavior of EBF links constructed of ASTM A992 steel", *J. Construct. Steel Res.*, **63**(6), 751-765. https://doi.org/10.1016/j.jcsr.2006.08.004.

Speicher, M.S. and Iii, J.L.H. (2016), "Collapse prevention seismic performance assessment of new eccentrically braced frames using ASCE 41", *Eng. Struct.*, **117**(6), 344-357. https://doi.org/10.1016/j.engstruct.2016.02.018.

Tian, X.H., Su, M.Z., Lian M., Wang, F. and Li, S. (2018), "Seismic behavior of k-shaped eccentrically braced frames with high-strength steel: shaking table testing and FEM analysis", *J. Construct. Steel Res.*, **143**(4), 250-263. https://doi.org/10.1016/j.jcsr.2017.12.030.

Wang, F., Su, M.Z., Hong, M., Guo, Y., and Li, S.H. (2016), "Cyclic behaviour of y-shaped eccentrically braced frames fabricated with high-strength steel composite", *J. Construct. Steel Res.*, **120**(4), 176-187. https://doi.org/10.1016/j.jcsr.2016.01.007.